Heated Polar Caps in PSRs 0656+14 and 1055–52

C. Greiveldinger, U. Camerini, W. Fry, C. B. Markwardt, H. Ögelman, S. Safi-Harb
Department of Physics, University of Wisconsin–Madison, 1150 University Avenue, Madison, WI 53706

J. P. Finley
Purdue University 1396 Physics Building, West Lafayette, IN 47907-1396

S. Tsuruta
Department of Physics, Montana State University, Bozeman, MT 59717

and

S. Shibata, T. Sugawara, S. Sano, M. Tukahara
Department of Physics, Yamagata University, Yamagata 990, Japan

ABSTRACT

We present new ASCA observations covering the 0.5 to 10 keV X-ray range of the cooling neutron star candidates PSR 0656+14 and PSR 1055–52. Previous ROSAT observations had shown that two component models, either two blackbodies or a blackbody plus a power-law, provided the best spectral fits to their X-ray emission. The combined ASCA and ROSAT spectrum of PSR 0656+14 reveals two blackbody components with T$\approx 8\times10^5$K and T$\approx 1.5\times10^6$K and shows evidence that a power-law component is needed to account for higher energy photons. This three component fit gives a reduced χ^2 that is half the value of a more conventional two component fit (1.3 as compared to 2.4). The fit to the combined spectrum for PSR 1055–52 yields a two blackbody fit with T$\approx 8 \times 10^5$K and T$\approx 3.7 \times 10^6$K. Our results favor the existence of a hot polar cap in each of these pulsars with the ratio of the polar cap area to the neutron star surface area being 7×10^{-3} and 3×10^{-5} for PSR 0656+14 and PSR 1055–52, respectively. The results are compared to models that make predictions of polar cap heating processes.

Subject headings: pulsars: general—pulsars: individual (PSR 0656+14, PSR 1055–52)—stars: neutron

1. Introduction

X-ray emission from pulsars is generally explained in one of three ways: thermal emission from the entire surface, thermal emission from a hot polar cap, or power-law emission from the pulsar magnetosphere. ROSAT observations of the pulsars PSR 0656+14 (Finley, Ögelman, & Kızıloğlu 1992), Geminga (Halpern & Ruderman 1993), PSR 1055–52 (Ögelman & Finley 1993), and the Vela pulsar (Ögelman, Finley, & Zimmerman 1993) have revealed spectra that are combinations of the surface thermal emission plus one of the other mechanisms. The limited energy range of ROSAT makes it difficult to constrain the parameters of the hard components of these neutron stars. In this letter we present the details of the ASCA observations of PSR 0656+14 and PSR 1055–52 (see Table 1). Then we explain the spectral and timing analysis, and finally we discuss the consequences of these results.

2. Observations and Results

The ASCA observation of PSR 0656+14 took place from 1994 March 31 to 1994 April 1, and the observation of PSR 1055–52 was done on 1995 January 18. The two ASCA Solid State Imaging Spectrometers (SIS) are X-ray CCD cameras in the focal planes of two of the four telescopes on the ASCA satellite (Tanaka, Inoue, & Holt 1994). For these observations two CCDs were activated for each SIS, giving a rectangular 11×22 arcmin^2 field of view. In the focal planes of the other two telescopes are the ASCA Gas Imaging Spectrometers (GIS), which are imaging gas scintillation proportional counters with 50 arcmin diameter circular fields of view. After removing times of high particle background rate, we were left with SIS exposure times of 30 ks for PSR 0656+14 and 27 ksec for PSR 1055-52. To achieve 1 ms timing accuracy we selected GIS data accumulated at high bit rate. This limited the GIS exposure time to 19 ks for both pulsars.

2.1. Spectral

The SIS data were selected from large circles (r=3 arcmin) centered on the locations of the pulsars. The particular sizes were chosen so that the extraction ring did not cross over CCD chip boundaries. To test for spectral fit sensitivity to background selection, various background regions from a given chip were used. Due to uncertainties in the low energy response of the SIS, photons with energies below 1 keV were discarded. Energies above 5 keV were dominated by background emission. In the 1 to 5 keV energy range, the same spectral model provided the best fit for all background regions tested. The background subtracted SIS count rate for PSR 0656+14 was $6.7 \pm 0.6 \times 10^{-2}$ c/s, and PSR 1055–52 was detected at $7.1 \pm 1.3 \times 10^{-3}$ c/s. For a given pulsar the spectra from both SIS detectors were fit simultaneously with the ROSAT spectrum using XSPEC v9.00.

Guided by the original ROSAT results, our initial spectral models were two component spectra composed of two blackbodies or a blackbody plus a power-law. These two component fits to PSR 0656+14 did not yield acceptable results (for these fits $\chi^2_\nu > 2$), so three component models were used. The best spectral fit was provided by two blackbodies plus a power-law with the parameters found in Table 2. The power-law fits a relatively flat high energy excess that extends to $\sim$5 keV, above which the spectrum is background dominated (Fig. 1). Our interpretation of the spectrum is that the soft blackbody component is produced by thermal emission from the neutron star surface; the hard blackbody comes from a reheated polar cap, and the power-law is produced by magnetospheric emission.

From the fluxes and temperatures for the two blackbody components listed for PSR 0656+14 in Table 2 we calculate the best-fit ratio of the high temperature area to the low temperature area $A_h/A_s = 7 \times 10^{-3}$, and the 1σ range is between 2×10^{-3} and 4×10^{-2}. Assuming a distance of 500 pc to PSR 0656+14 we derive a neutron star radius of 17^{+9}_{-3} km and a high temperature emitting area of $2.5^{+7.9}_{-1.7} \times 10^{11}$ cm^2. Both these areas are those determined by an observer at infinity.

Recently, Ramanamurthy et al. (1996) have presented evidence for high-energy γ-ray emission from PSR 0656+14. Their spectral parameters for photon energies greater than 100 MeV are $\alpha = 2.8 \pm 0.3$ and a number flux $4.1 \pm 1.4 \times 10^{-8}$ photons cm^{-2} s^{-1} and are marginally compatible with the power-law we detect if extended to γ-rays and is probably a result of outer gap emission. The possibility of an unresolved nebula cannot be ruled out, though.

Two component spectral fits, as found with ROSAT, work well to describe the spectrum of PSR 1055–52. Both a two blackbody spectrum and a blackbody plus power-law spectrum fit the data well. We prefer the two blackbody model because the best-fit power-law spectral index of 3–4 is larger than has been seen in pulsars, and the hard blackbody temperature is similar to that for PSR 0656+14. The temperatures and fluxes for the two components are indicated in Table 2. The ratio A_h/A_s has a best-fit value of 3×10^{-5} and lies between 6×10^{-6} and 3×10^{-4}. At a distance of 1 kpc the observed neutron star radius is 18^{+15}_{-4} km, and the hotter area is $1.1^{+8.2}_{-1.0} \times 10^9$ cm^2.

Naively we expect that the spectrum for PSR 1055–52 is due to the same processes that produce the spectrum of PSR 0656+14. The absence of the magnetospheric power-law component for PSR 1055-52 can be explained by the fact that there were nearly half the photons for this source than for PSR 0656+14. Therefore, any power-law extension would not rise significantly above the background level. It is possible to add the power-law spectrum from the EGRET fits (Fierro et al. 1993) and produce an acceptable χ^2, but the data does not require such an addition.

2.2. Timing

X-ray pulsations have been previously detected with ROSAT for both PSR 0656+14 and PSR 1055–52. Using ROSAT PSPC data Finley, Ögelman, & Kızıloğlu (1992) showed that PSR 0656+14 was pulsed at the radio period, and Ögelman (1995) showed that the pulsed fraction varied over the 0.1 to 2.4 keV energy range nearing a pulsed fraction of 20% at the highest energies. Similar behavior was found in the ROSAT PSPC data for PSR 1055–52 (Ögelman & Finley 1993). Between 0.1 and 2.4 keV the pulsed fraction varied from 8% to 80% and settled to 40% at higher energies.

In high bit rate mode the GIS data provided the time resolution ($\sim$ 1 ms) necessary to perform timing analysis. GIS photons were extracted from a 6 arcminute radius circle centered on the pulsar. We estimated the number of background photons that would be expected to fall in this region by sampling areas that are the same off-axis distance as the pulsar (5 arcmin). The number of background photons was 1031 ± 32, and the region centered on the pulsar yielded 1300 photons, corresponding to an 8σ excess. The same technique was employed for PSR 1055–52 and 1083 photons were extracted from a background of 954 ± 31, resulting in a 4σ excess.

The source photon arrival times were then corrected to the solar system barycenter using the JPL DE200 ephemeris. Each photon from PSR 0656+14 was phase related to the radio ephemeris shown in Table 1 (Arzoumanian et al. 1992), and thus the data were folded at the radio frequency. Using the Z_1^2 statistic (Buccheri et al. 1983) on the entire PSR 0656+14 GIS dataset (0.5-10 keV) we can place a 3σ upper limit on the pulsed fraction of 71%. The dataset was then divided into middle (0.5-2 keV) and high (2-10 keV) energy bins that had approximately equal numbers of photons (630 and 670, respectively). The middle energies were chosen as the energy range where the hard blackbody would be dominant, and pulsations were detected at a 2σ level with a pulsed fraction of $31 \pm 10\%$ (Figure 2). The Z_1^2 value for the high energy photons was too low (2.1) to derive a pulsed fraction, and because this energy regime was dominated by background photons, the 3σ upper limit approaches 100%.

PSR 1055–52 was analyzed according to the ephemeris shown in Table 1 (Kaspi et al. 1994). For the entire energy range, we determine that the 3σ upper limit on the pulsed fraction is 87%. The middle energy photons (0.5-2 keV, 460 photons) show pulsations at a significance of 2σ that yields a pulsed fraction 93^{+7}_{-32}% (Figure 2). The higher energies (2-10 keV, 600 photons) gave a $Z_1^2 = 0.5$ and suffered from the same background dominated difficulties as PSR 0656+14, and again, the 3σ pulsed fraction upper limit nears 100%.

Compared with the lower energy ROSAT results, the increase in the amplitude of pulsations in the energy range where the hard blackbody is dominant is consistent with emission from a hot polar cap that rotates through our line of sight. The pulse phases from ASCA are also consistent with the hard ROSAT band, although the significance of the ASCA data renders the phase determination ambiguous. With better photon statistics in this energy range we would be able to use the pulsation amplitude and relativistic light deflection considerations to constrain the radius of the neutron star (Yancopolous, Hamilton, & Helfand 1994).

3. Discussion and Conclusions

The soft blackbody components we detect are consistent with the ROSAT results (Ögelman 1995, Ögelman & Finley 1993, Finley et al. 1992) and are best interpreted as thermal emission from the entire surface of a cooling neutron star (Nomoto & Tsuruta 1987). The harder component on which we focus in this paper can be partly due to more detailed neutron star atmosphere models (Pavlov et al. 1994). However, certain specific models have been compared to ROSAT data and found to be unacceptable (Ögelman and Finley 1993, Greiveldinger et al. 1994). When interpreted as blackbody emission, the hard component emanates from an area that is much smaller than that of the soft blackbody component; a natural explanation for this would be the presence of a heated polar cap.

In general, the energy deposited in the polar cap is dependent on the current flowing in and the voltage across the accelerator. The current is difficult to determine with local models (Shibata 1995), but it will be on the order of the Goldreich-Julian current density, $\frac{B_p\Omega}{2\pi e}$, where B_p is the magnetic field strength at the pole, and Ω is the angular frequency of the pulsar. The voltage across a polar cap accelerator will be $\approx 10^{12}$ V as determined by the breakdown potential (Ruderman & Sutherland 1975). Using the current density as determined from the parameters in Table 1 and the breakdown voltage, an upper limit to the polar cap temperature for PSR 0656+14 is 5×10^6 K, and 4×10^6 K for PSR 1055–52. For a 1.4$M_\odot$ star with a radius of 10 km the temperatures observed at infinity (T_∞) will be 4×10^6 K and 3×10^6 K for PSRs 0656+14 and 1055–52, respectively, which are close to the observed values.

The following models include effects that are ignored in the very simple analysis above, but they still predict temperatures that are the same order of magnitude as observed. The model of Cheng & Ruderman (1980) uses an ion plasma to moderate the voltage and current in the acceleration region. The temperatures predicted from this model depend on the binding energy of ions in the neutron star surface, and these temperatures are a factor of four or more smaller than our rough estimates. The slot-gap model of Arons (1981a) provides a more detailed treatment of the geometry of the acceleration region and predicts $T_\infty \approx 2.0 \times 10^6$ K for both pulsars, in accordance with our observations.

The model of Halpern & Ruderman (1993) to explain the ROSAT spectrum of Geminga invokes the outer magnetospheric gap accelerators. The accelerating voltages in the outer gaps are larger than those in the polar caps, but as electrons travel from the inner edge of the gap to the stellar surface they lose some energy through radiation. One can determine how much energy an electron will deposit in the polar cap and then determine the maximum temperature that will be seen by using the Goldreich-Julian current density. The maximum temperatures expected are: T_∞(PSR 0656+14)=5.4×10^6K and T_∞(PSR 1055–52)=4.3×10^6K. Even though a different acceleration region is used in this model, these upper limits are consistent with the measured temperatures for these two pulsars.

To make predictions for an expected luminosity, the geometry of the polar cap must be assumed. The canonical polar cap radius is given by $r_c = R(\Omega R/c)^{1/2}$, where R is the neutron star radius (Beskin, Gurevich, & Istomin 1993), and the three models discussed use this radius, to within a factor of ~ 2, to calculate luminosities. The ratio of the polar cap area to the neutron star surface area is $\frac{\Omega R}{4c}$. For a neutron star radius of 10 km and values of Ω similar to these pulsars, this ratio is $\sim 10^{-4}$, consistent with the value seen for PSR 1055–52, but smaller than that for PSR 0656+14 by at least a factor of 15.

There have been detections of hot polar cap emission from other pulsars. Since no softer thermal component from the entire stellar surface was detected from the following sources, we will assume a neutron star radius of 10 km to compare with our results. Becker & Trümper (1993) detected thermal emission from the 6 ms pulsar PSR J0437-4715 emanating from an area that is $\approx 4 \times 10^{-5}$ of the stellar surface area. Yancopoulos et al. (1994) detected thermal X-ray emission from PSR 1929+10 and determine, in the simple analysis that we have followed, that the polar cap area is $\approx 2 \times 10^{-6}$ that of the stellar area. With Geminga, Halpern & Ruderman (1993) detected emission from both the stellar surface and the polar cap, and the polar cap surface area is $\approx 3 \times 10^{-5}$ that of the stellar area. For these pulsars the ratio of cap to stellar area is below that expected, which is $\approx 10^{-4}$ except for PSR J0437-4715 where the expected ratio is $\approx 10^{-2}$.

There are various other factors that may have bearing on our comparison of observed polar cap size to the theoretical size. The different angles at which we observe the rotating polar caps would cause a difference in the derived polar cap radii. Arons (1981b) allows for the possibility that the polar cap could be larger than that due to a pure dipole. It is also possible that only a portion of the polar cap would be bombarded by electrons to reheat it (Arons 1981a) serving to make the area smaller, and Halpern & Ruderman (1993) argue that for their outer magnetospheric gap model to be consistent with the Geminga data an off-axis dipole is needed. It is conceivable that the right combination of viewing angle, inclination angle between rotation and dipole axes, and deviation from dipolar magnetic geometry may explain the differing polar cap sizes.

The power-law portion of the PSR 0656+14 spectrum is most likely due to magnetospheric emission. The Crab pulsar, PSR 0540–69 and PSR 1509–58 are dominated by their magnetospheric processes with power-law photon indices ranging from 1.1 (PSR 1509-58, Greiveldinger et al. 1995) to 2.4 (PSR 0540-69, Finley et al. 1993). The value α = 1.5 for PSR 0656+14 is consistent with this range. For a distance of 500 pc, the luminosity of the power-law component from 0.1 to 2.4 keV is 4.1×10^{30} erg s^{-1}, and the empirical model for magnetospheric X-ray emission of Ögelman (1995) predicts a similar luminosity of 7.4×10^{30} erg s^{-1} in this energy range.

Earlier discussion of the excess hard emission discovered in neutron stars considered either a hot polar cap source or a magnetospheric origin. Our results for PSR 0656+14 give evidence that both components may be present. Magnetospheric processes are in fact used to explain the polar cap heating mechanism, and it is not surprising that there is spectral evidence of these processes.

This work was supported by NASA grants NAG5-2557, NAGW-2643, and NAGW-2208.

Table 1.
Pulsar Parameters

	PSR 0656+14	PSR 1055–52
f_0 (Hz)	2.5981686189472	5.0732940338018
$\dot{f}$ (Hz s^{-1})	-3.71356×10^{-13}	-1.50096×10^{-13}
Epoch	2448731.500000950	2449481.500001127
$\dot{E}$(erg s^{-1})	3.8×10^{34}	3.0×10^{34}
τ(years)	1.1×10^{5}	5.4×10^{5}
B(Gauss)	4.7×10^{12}	1.1×10^{12}

Timing data from Arzoumanian, Nice, & Taylor (1992), and Kaspi et al. (1994).

Table 2.

Spectral fits to the combined ROSAT PSPC and ASCA SIS data. Errors are quoted at the 1σ level.

Spectral Component	PSR 0656+14	PSR 1055–52
$N_H(\times 10^{20}$ cm$^{-2})$	$1.7^{+0.4}_{-0.2}$	2.6 ± 0.6
T_s(K)	$7.8^{+0.5}_{-1.4} \times 10^{5}$	$7.9^{+0.6}_{-1.0} \times 10^{5}$
f_s(erg cm^{-2} s^{-1})	$2.4^{+0.2}_{-0.3} \times 10^{-11}$	$7.8^{+7.0}_{-2.0} \times 10^{-12}$
T_h(K)	$1.5 \pm 0.2 \times 10^{6}$	$3.7^{+2.0}_{-1.2} \times 10^{6}$
f_h(erg cm^{-2} s^{-1})	$2.4^{+1.7}_{-1.2} \times 10^{-12}$	$1.0^{+0.7}_{-0.3} \times 10^{-13}$
α	1.5 ± 1.1	–
A^a	$3.5^{+6.1}_{-2.7} \times 10^{-5}$	–

[a] photons cm^{-2} s^{-1} keV^{-1} at 1 keV

REFERENCES

Arons, J. 1981a, in Pulsars (IAU Symposium No. 95), ed W. Sieber and R. Wielebinski (Dordrecht: Reidel), 69

Arons, J. 1981b, ApJ, 248, 1099

Arzoumanian, Z., Nice, D., Taylor, J. H. 1992, GRO/radio timing data base, Princeton University

Becker, W. & Trümper, J. 1993, Nature, 365, 528

Beskin, V. S., Gurevich, A. V., & Istomin, Ya. N. 1993, Physics of the Pulsar Magnetosphere (Cambridge: Cambridge University Press), 117

Buccheri, R., et al. 1983, A&A, 128, 245

Cheng, A. F. & Ruderman, M. A. 1980, ApJ, 235, 576

Fierro, J. M. et al. 1993, ApJ, 413, L27

Finley, J. P., Ögelman, H., Hasinger, G., & Trümper, J., 1993, ApJ, 410, 323

Finley, J. P., Ögelman, H. & Kızıloğlu, Ü. 1992, ApJ, 394, L21

Greiveldinger, C., Markwardt, C., Ögelman, H., Safi-Harb, S., & Finley, J. P. 1994, BAAS, 184, # 8.01

Greiveldinger, C., Caucino, S., Massaglia, S., Ögelman, H., & Trussoni, E. 1995, ApJ, 454, 855

Halpern, J. P. & Ruderman, M. 1993, ApJ, 415, 286

Kaspi, V. M., Manchester, R. N., Bailes, M., D'Amico, N.,

Lyne, A. G. 1994, GRO/radio timing data base, Princeton University

Nomoto, K., & Tsuruta, S. 1987, ApJ, 312, 711

Ögelman, H. 1995, in Proc. NATO ASI on the Lives of Neutron Stars, ed. A. Alpar, Ü. Kızıloğlu, & J. van Paradijs (Dordrecht: Kluwer), 101

Ögelman, H. & Finley, J. P. 1993, ApJ, 413, L31

Ögelman, H., Finley, J. P. & Zimmermann, H. U. 1993, Nature, 361, 136

Pavlov, G. G., Shibanov, Yu. A., Ventura, J., & Zavlin, V. E. 1994, A&A, 289, 837

Ramanamurthy, P. V., Fichtel, C. E., Kniffen, D. A.,

Sreekumar, P., & Thompson, D. J. 1996, ApJ, 458, 755

Ruderman, M. A., & Sutherland, P. G. 1975, ApJ, 196, 51

Shibata, S. 1995, MNRAS, 276, 537

Tanaka, Y., Inoue, H., & Holt, S. S. 1994, PASJ, 46, L37

Yancopoulos, S., Hamilton, T. T., & Helfand, D. J. 1994, ApJ, 429, 832

This preprint was prepared with the AAS LATEX macros v3.0.

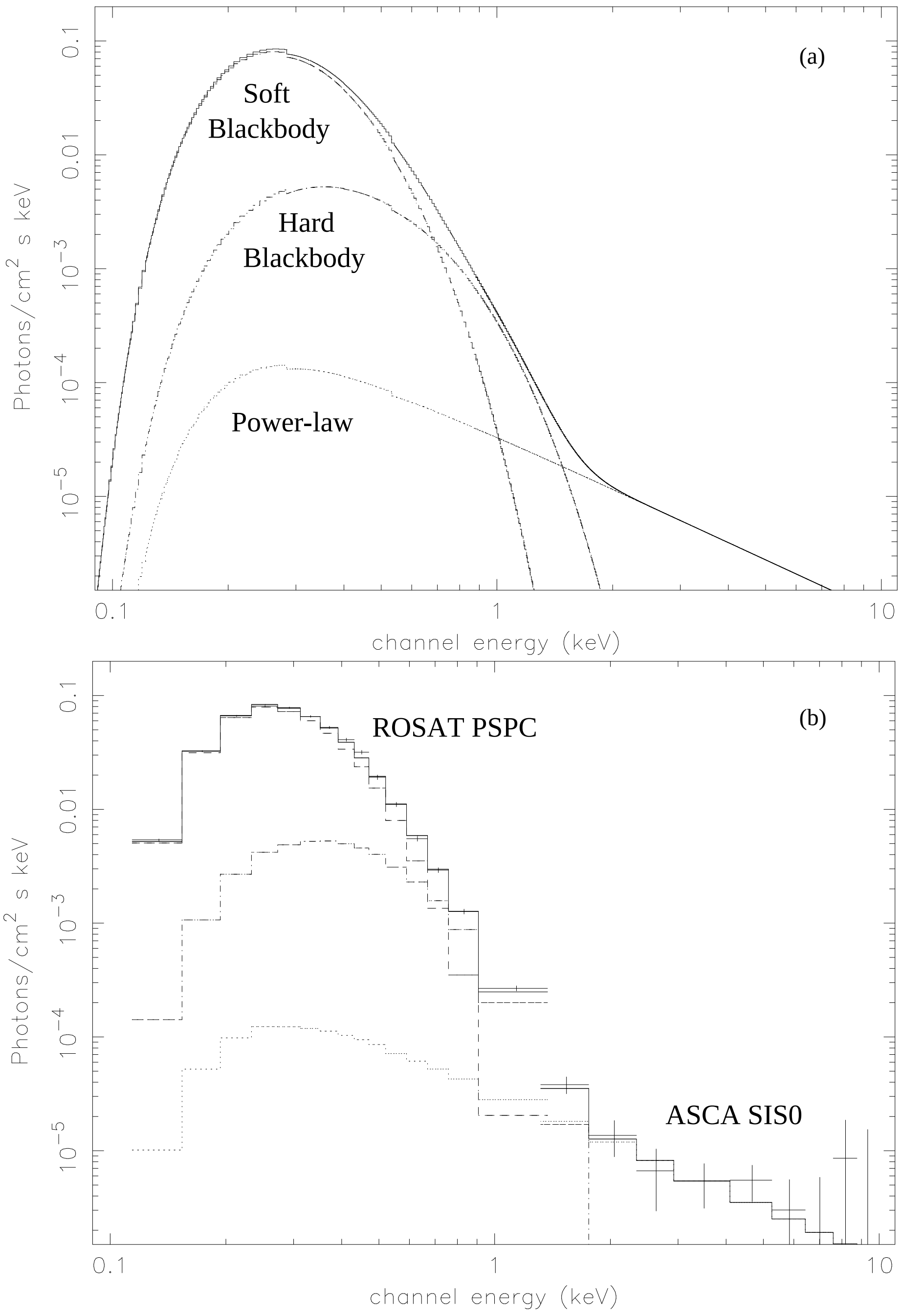

Fig. 1.— Modeled spectrum of PSR 0656+14. The incident spectrum (a) consists of a soft blackbody component that is emitted from the entire neutron star surface, a hard blackbody component that is radiated from the reheated polar cap, and a power-law extension from magnetospheric processes. In (b) the unfolded data and model spectral components are shown. For clarity, overlapping energy bins are removed and data from only a single SIS camera is shown.

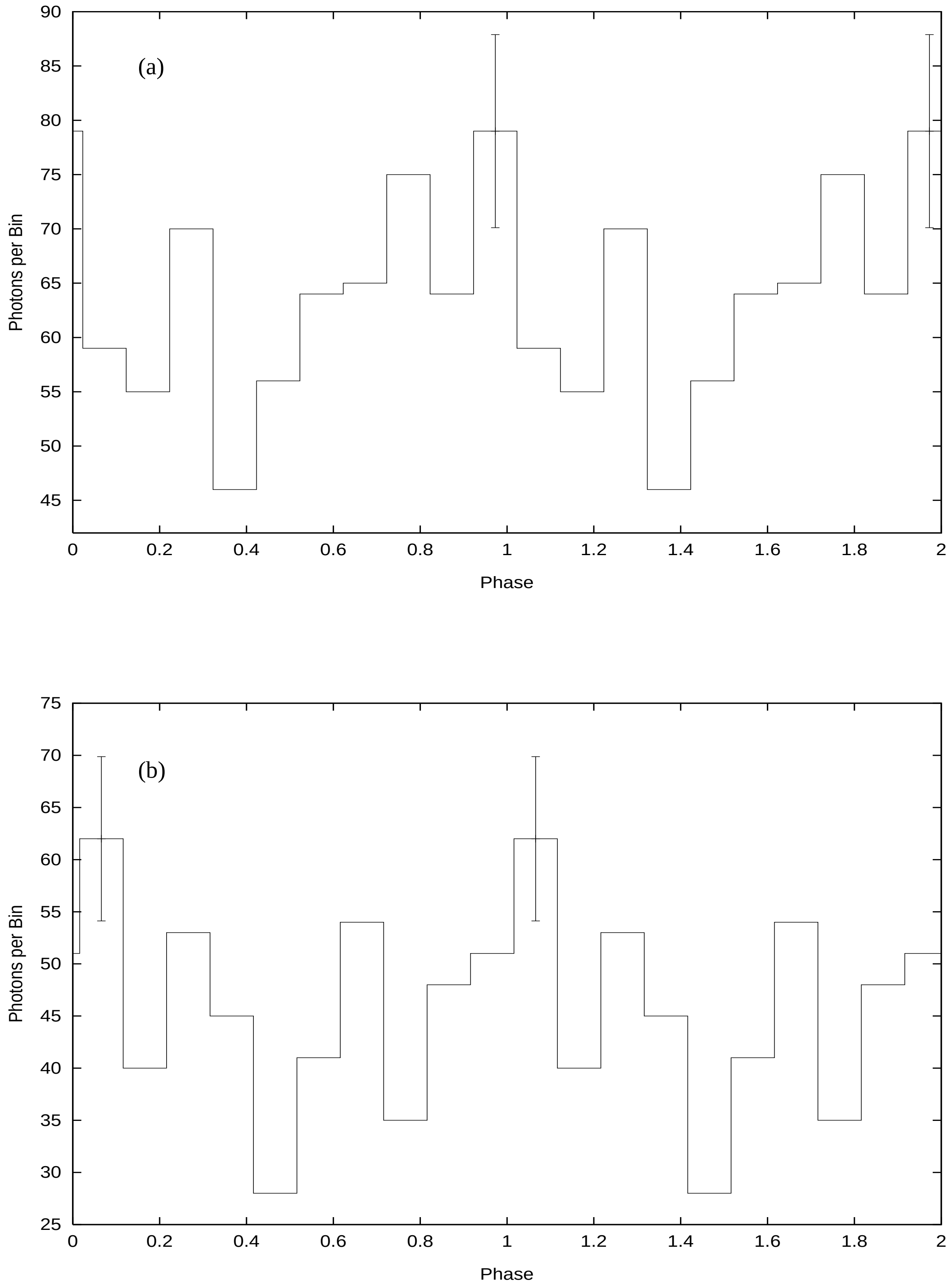

Fig. 2.— Pulse shapes from 0.5 to 2 keV ASCA GIS data for (a) PSR 0656+14 and (b) PSR 1055–52. The data is referenced to the radio phase, and two pulse periods are shown for clarity.